Half-sandwich manganese complexes Cp(CO) 2 Mn(NHC) as redox-active organometallic fragments

Rémy Brousses, Vincent Maurel, Jean-Marie Mouesca, Vincent César, Noël Lugan, Dmitry A. Valyaev

Half-sandwich manganese complexes $Cp(CO)_2Mn(NHC)$ as redox-active organometallic fragments

Rémy Brousses,[a] Vincent Maurel,[b] Jean-Marie Mouesca,*[b] Vincent César,[a] Noël Lugan*[a] and Dmitry A. Valyaev*[a]

Oxidation of the half-sandwich Mn^{I} complexes $Cp(CO)_2Mn(NHC)$ bearing dialkyl-, arylalkyl- and diarylsubstituted N-heterocyclic carbene ligands (NHC = IMe, IMeMes, IMes) affords the corresponding stable Mn^{II} radical cations $[Cp(CO)_2Mn(NHC)](BF_4)$ isolated in 92-95% yield. Systematic X-ray diffraction study of the series of Mn^{I} and Mn^{II} NHC complexes revealed the expected characteristic structural changes upon oxidation, namely the elongation of Mn–CO and Mn–NHC bonds as well as the diminution of OC–Mn–CO angle. ESR spectra of $[Cp(CO)_2Mn(IMes)](BF_4)$ in frozen solution (CH_2Cl_2/toluene 1:1, 70K) allowed the identification of two conformers for this complex and their structural assignment using DFT calculations. The stability of these NHC complexes in both metal oxidation states, moderate oxidation potentials and the ease of detection of Mn^{II} species by a variety of spectroscopic techniques (UV-Vis, IR, paramagnetic ^1H NMR, and ESR) make these compounds promising objects for applications as redox-active organometallic fragments.

Introduction

Organometallic complexes possessing two distinct stable oxidation states are widely used as redox-active fragments in many areas of chemistry providing numerous applications in molecular recognition,[1] electrode surface modification,[2] design of electroactive polymers[3] and molecular machines,[4] as well as in redox-switchable homogeneous catalysis.[5,6] Most of the systems are based on ferrocene (Fc) derivatives (Chart 1, (a)) owing to the perfect electrochemical reversibility of the Fe^{II}/Fe^{III} couple,[7] the remarkable stability of the 17-electron Fc^+ radical cations, and the structural diversity available from well-developed synthetic Fc chemistry.[8] In parallel, C. Lapinte and coll. showed that the electron-rich half-sandwich iron diphosphine complexes [Cp*(dppe)FeX] (Chart 1, (b)) can be also used as efficient redox-active units.[9]

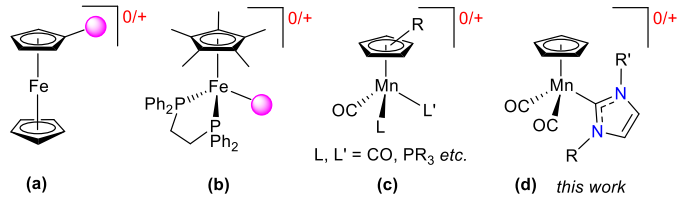

Chart 1. Organometallic complexes as redox-active moieties

In contrast to above extensively studied iron complexes-based systems, the potential application of related 18-electron half-sandwich manganese complexes as redox tags has been far less developed. Though cymantrene, $[CpMn(CO)_3]$ (Chart 1, (c), L = L' = CO, R = H), can be reversibly oxidized under cyclic voltammetry (CV) conditions,[10] albeit at much higher potentials than Fc ($E_{1/2}$ = +0.92 V *vs.* Fc/Fc^+),[10c] the corresponding radical cation could be isolated and fully characterized only upon association with a non-nucleophilic counter-anions, namely $B(C_6F_5)_4^-$.[10c] The introduction of electron-donating groups into the Cp ring,[10c,11] or the substitution of one[12] or two[13] carbonyl ligands for less π-accepting ligands, including MeCN, amines, isonitriles, phosphites, or phosphines, decreased as expected the Mn^{I}/Mn^{II} oxidation potentials down to –0.05 V *vs.* Fc/Fc^+ for $[Cp(dppe)Mn(CO)]$,[13] but the resulting radical cations were actually never isolated in a pure state.

We had initially observed that half-sandwich manganese complexes bearing backbone-substituted N-heterocyclic carbene (NHC) ligands (Chart 1, (d)) easily undergo a reversible one-electron oxidation under CV conditions at rather low potentials (–0.20 - –0.26 V *vs*. Fc/Fc^+).[14] Taking into account the well-established ability of NHC ligands to stabilize electron-deficient species,[15] we engaged into a systematic study of the electrochemical properties of a series $Cp(CO)_2Mn(NHC)$ complexes envisioning that the derived Mn^{I}/Mn^{II} couple could afford exploitable redox-active organometallic tags. While our work was in progress, W. E. Geiger and coll. reported in 2019 the synthesis and the structural study of a stable Mn^{II} complex bearing the bulky 1,3-bis(2,6-diisopropylphenyl)imidazol-2-ylidene (IPr) ligand, namely $[Cp(CO)_2Mn(IPr)](PF_6)$, showing such a goal was indeed achievable.[16] This prompts us to report now our own complementary studies on the preparation of a series of half-sandwich Mn^{II} complexes bearing different, less

[a] *LCC-CNRS, Université de Toulouse, CNRS, Toulouse, France*
E-mails: noel.lugan@lcc-toulouse.fr, dmitry.valyaev@lcc-toulouse.fr.
[b] *Univ. Grenoble Alpes, CEA, CNRS, INAC, SyMMES, F-38000 Grenoble, France*
E-mail: jean-marie.mouesca@cea.fr.

† Electronic Supplementary Information (ESI) available: Cyclic voltammograms for complexes **1-3**, copies of all original spectra for complexes [**1-3**]BF_4, Cartesian coordinates of DFT optimized structures and additional details on ESR spectra simulation. CCDC 1485213, 2092735-2092739. See DOI: 10.1039/x0xx00000x

sterically demanding NHCs ligands, their characterization by a complete set of spectroscopic methods, including paramagnetic NMR and state-of-the-art ESR spectroscopy when applicable, complemented by structural studies for the entire set of Mn^{I}/Mn^{II} couples.

Results and discussion

Synthesis and structural characterization of Mn^{II} NHC complexes $[Cp(CO)_2Mn(NHC)](BF_4)$

A representative series of half-sandwich Mn^{I} complexes $Cp(CO)_2Mn(NHC)$ (**1**-**3**, Scheme 1) bearing, respectively, dialkyl- (IMe), arylalkyl- (IMeMes), and diarylsubstituted (IMes) imidazol-2-ylidene ligands were prepared in good yield by photochemical substitution of one carbonyl group in cymantrene $[CpMn(CO)_3]$ for the corresponding free NHC according to a previously reported procedures.[14,17] Under CV conditions (Pt electrode, CH_2Cl_2, 0.1 M Bu_4NPF_6, 100 mV/s, SCE) all these compounds display perfectly reversible one-electron oxidation behavior (Figure S1). The oxidation potentials within the series decrease with the stepwise replacement of the methyl substituent(s) in the NHC ligand for mesityl one(s) ($E_{1/2}$: –0.225 (**1**), –0.266 (**2**), –0.297 (**3**) V *vs.* Fc/Fc^{+}) comforting the stronger electron donating properties of IMes compared to IMe as shown earlier on the basis of IR analysis.[18]

The chemical oxidation of the Mn^{I} complexes **1-3** with one equivalent of $[Fc](BF_4)$ proceeds rapidly at room temperature to afford the corresponding $[Cp(CO)_2Mn(NHC)](BF_4)$ ($[\mathbf{1\text{-}3}](BF_4)$) being isolated in high yield upon simple precipitation with ether (Scheme 1). Solid state squid measurements for $[\mathbf{1\text{-}3}]BF_4$ revealed magnetic moments of 1.7-2.2 μ_B consistent with the formation of low-spin (S = ½) Mn^{II} complexes. These experimental observations were corroborated by DFT study revealing the Mulliken spin population at the metal atom to be close to unity and slightly decreasing for bulkier NHC ligands (1.09, 1.04 and 1.01 for $[\mathbf{1}]^+$, $[\mathbf{2}]^+$ and $[\mathbf{3}]^+$, respectively). The SOMO orbitals of $[\mathbf{1\text{-}3}]^+$ (Figure S2) are mainly localized at the metal center and in some extent at the NHC ligand being consistent with previously reported data.[14,16] Once purified, the present 17-electron Mn^{II} derivatives are stable in the solid state under ambient conditions for several days but they are sensitive to oxygen in solution. Noticeably, the thermal stability of complex $[\mathbf{1}](BF_4)$ bearing one of the less bulky NHC ligands[19] shows that the steric protection in this case is less important than the electronic stabilization.

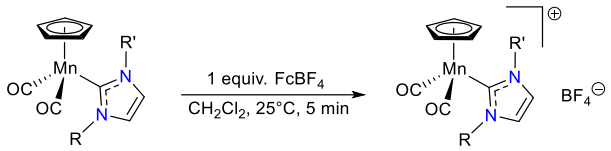

1 R = R' = Me — $[\mathbf{1}](BF_4)$ 94%
2 R = Me; R' = Mes — $[\mathbf{2}](BF_4)$ 95%
3 R = R' = Mes — $[\mathbf{3}](BF_4)$ 92%

Scheme 1. Synthesis of Mn^{II} NHC complexes $[\mathbf{1\text{-}3}](BF_4)$

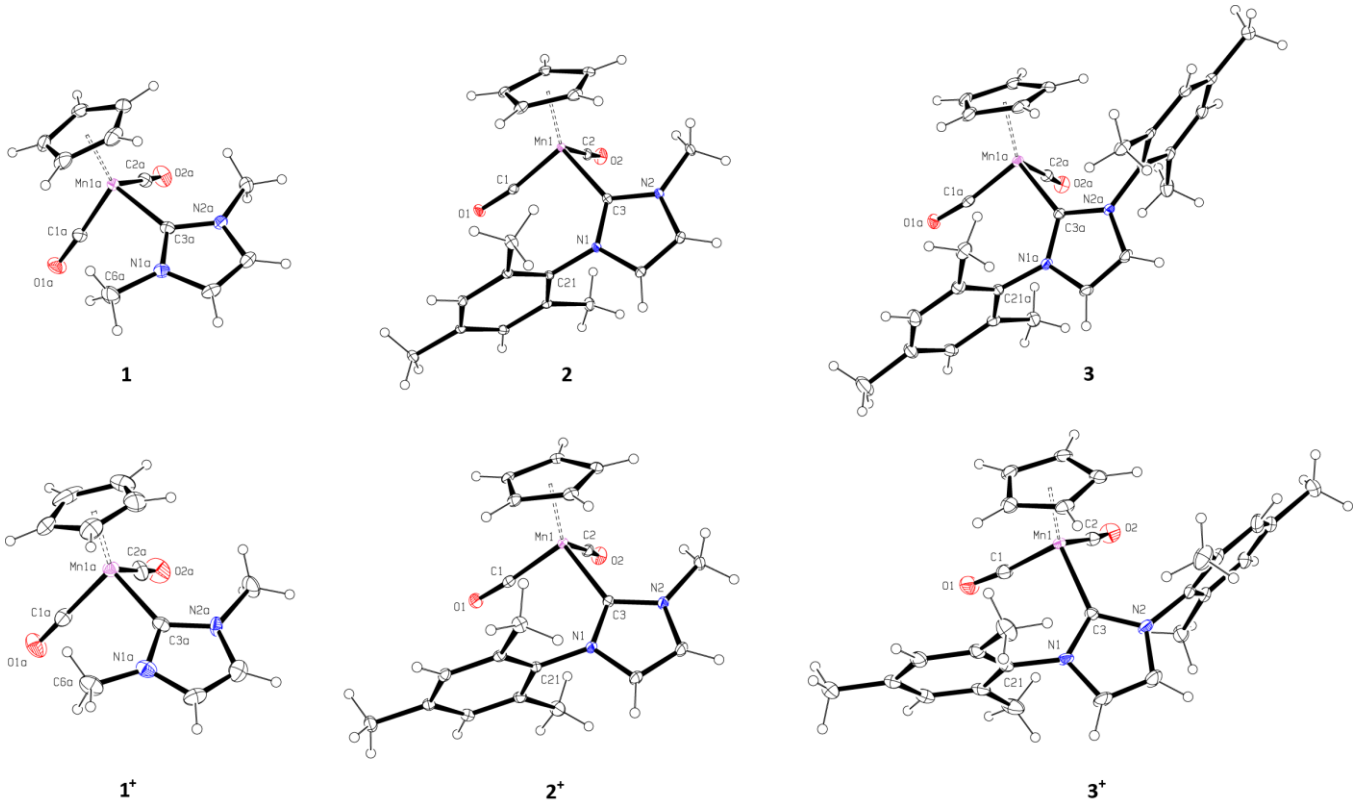

Figure 1. Perspective view of Mn^{I} complexes $[Cp(CO)_2Mn(NHC)]$ **1-3** (upper row) and their Mn^{II} radical cations $[Cp(CO)_2Mn(NHC)](BF_4)$ $[\mathbf{1\text{-}3}](BF_4)$ (lower row). Ellipsoids are set on 30% probability and BF_4^- anions for cationic products are not shown. For compounds **1**, $[\mathbf{1}](BF_4)$ and **3** containing several crystallographically independent molecules in the cell only the parts A are presented.

Table 1. Selected bond lengths (Å) and angles (°) for Mn^{I} and Mn^{II} NHC complexes $[Cp(CO)_2Mn(NHC)]^{0/+}$

Complex	**1**[a]	[**1**](BF$_4$)[a]	**2**	[**2**](BF$_4$)	**3**[b]	[**3**](BF$_4$)
Mn1–C3	1.989(3)	2.011(4)	1.9971(12)	2.0270(14)	2.007(3)	2.019(3)
Mn1–Cp$_{cnt}$	1.7827(4)	1.7790(10)	1.78451(19)	1.7921(6)	1.786(2)	1.7850(5)
Mn1–Cp [c]	2.148	2.140	2.147	2,161	2.152	2.158
Mn1–C1	1.763(3)	1.848(10)	1.7618(13)	1.8439(14)	1.762(3)	1.825(3)
Mn1–C2	1.759(3)	1.818(11)	1.7679(14)	1.8348(17)	1.756(3)	1.847(3)
C1–O1	1.165(4)	1.117(12)	1.1652(17)	1.1413(17)	1.170(4)	1.154(4)
C2–O2	1.157(4)	1.153(13)	1.1638(17)	1.1419(18)	1.172(4)	1.139(4)
C1–C6	3.246(5)	3.200(15)	–	–	–	–
C1–C21	–	–	2.9016(17)	3.1297(19)	2.883(2)	3.175(4)
Mn1–C1–O1	175.6(3)	177.2(10)	171.41(11)	173.94(11)	170.2(3)	174.7(3)
Mn1–C2–O2	176.3(3)	178.4(10)	175.15(11)	175.55(12)	174.8(3)	175.7(3)
C1–Mn1–C2	88.09(14)	84.4(2)	90.34(6)	81.93(6)	87.40(14)	84.22(15)
Cp$_{cnt}$–Mn1–C3–N2	–92.01(25)	–88.84(12)	–62.48(12)	–74.11(12)	–54.7(1)	–82.94(26)
N1–C3–Mn1–C1	–53.52(27)	49.46(58)	–20.75(12)	–39.12(12)	6.71(33)	–43.30(68)

[a] Two independent molecules were found in the cell having similar metrical data within experimental error (the values for the molecule A are given)
[b] Four independent molecules were found in the cell having similar metrical data within experimental error (the values for the molecule A are given)

The molecular structures of Mn^{II} complexes [**1-3**](BF$_4$) and their parent Mn^{I} precursors **1-3**[20] were determined by X-ray diffraction (Figure 1). The most pertinent metrical data are gathered in the Table 1. While Mn–Cp bond distances remain marginally affected upon oxidation, other metal-ligand bonds in the cationic [**1-3**](BF$_4$) species appear to be significantly elongated as compared to their neutral counterpart, this beingparticularly noticeable for the Mn–CO bonds being longer by 0.06-0.08 Å, as previously observed in the parent $[Cp(CO)_2Mn(IPr)](PF_6)$ complex.[16] This observation together with the systematic shortening of C≡O bonds is fully consistent with the expected reduced π-backbonding in the 17-electron NHC complexes as compared to their 18-electron congeners.[16,21] Also significant is the tightening of the OC–Mn–CO angle in the [**1-3**](BF$_4$) series as compared to their neutral antecedent (C1–Mn1–C2, Table 1) being typically observed upon oxidation of dicarbonyl half-sandwich complexes.[22]

The structural analysis of the full set of Mn^{I} and Mn^{II} complexes revealed the orientation of the carbene ligands[23] is sensitive to both the presence of aryl groups at the nitrogen atoms of the NHCs and metal oxidation state (Figure 2). The IMe ligand in complex **1** adopts an almost ideal so-called 'horizontal' coordination mode[23] with a torsion angle Cp$_{cnt}$–Mn1–C3–N2 of –92.01(25)° being similar to that found in the structures of the isoelectronic $[Cp(CO)_2Cr(IMe)]^{-}$[21b] and $[Cp(CO)_2Fe(IMe)]^{+}$[24] analogues. Noticeably, in IMeMes and IMes Mn^{I} derivatives **2** and **3**, the NHC ligands adopt a conformation we denote 'eclipsed', by which the heterocycle is almost coplanar with one of the CO ligands (N1–C3–Mn1–C1 torsion angle, Table 1). This conformation brings one of the mesityl group in the vicinity of one of the carbonyl ligands, namely C1O1, the associated C_{ipso}...C≡O distance (C1–C21, Table 1) being inferior to the sum of the corresponding van der Vaals radii (3.2 Å), and induces a significant bending of the corresponding Mn–C–O fragment (Mn1–C1–O1, Table 1). Such structural features are thought to be indicative of the development of a weak intramolecular attractive interaction involving the given Mes group and CO ligand through a $\pi(C{=}C)_{Mes} \rightarrow \pi^*(C{\equiv}O)$ donation as previously identified in half-sandwich Mn^{I} and Fe^{II} carbene complexes.[25] While a minimal conformational change is observed for the IMe ligand for the couple **1** / [**1**](BF$_4$), the NHC ligands in [**2**](BF$_4$) and [**3**](BF$_4$) now show an almost horizontal coordination mode (Figure 2, Cp$_{cnt}$–Mn1–C3–N2: –74.11(12)° for [**2**](BF$_4$), –82.94(26)° for [**3**](BF$_4$)). With such an orientation, the C_{ipso}...C≡O distances are now close to the sum of the van der Waals carbon radii (C1–C21, Table 1) while the Mn–C≡O angles becomes typical (Mn1–C1–O1 Table 1). This suggests that the attractive $\pi(C{=}C)_{Mes} \rightarrow \pi^*(C{\equiv}O)$ intramolecular interaction identified in the structure the neutral species is no longer operative – or at least no more dominant – in the radical cations, in the solid state. This might be due to the combination of the intrinsic global extension on the metal-ligands bonds and the tightening of the OC–Mn–CO angle (*vide supra*), setting *ipso facto* the mesityl(s) group(s) too far away from any of the carbonyl ligand(s) for establishing a determining interaction.

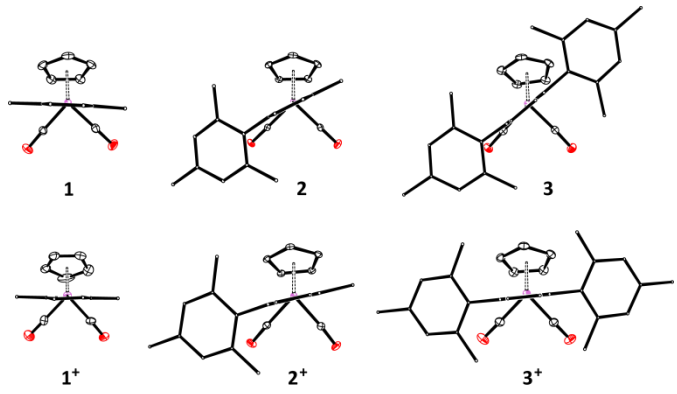

Figure 2. The orientation of the NHC ligands in Mn^{I} complexes **1-3** (upper row) and their Mn^{II} analogues [**1-3**](BF$_4$) (lower row, BF_4^- anions are not presented).

Spectroscopic investigation of Mn^{I} and Mn^{II} NHC complexes $[Cp(CO)_2Mn(NHC)]^{0/+}$

Solution IR spectra of complexes [**1-3**](BF$_4$) in CH_2Cl_2 display two expected intense ν_{CO} bands shifted to higher frequencies by 120-130 cm^{-1} relative to those of parent derivatives **1-3** (Table

Table 2. IR, UV-Vis spectroscopy and cyclic voltammetry data for NHC complexes $[Cp(CO)_2Mn(NHC)]^{0/+}$ (NHC = IMe, IMeMes, IMes, IPr)

Complex	IR, ν_{CO} (cm^{-1}) [a]	UV-Vis, λ nm (ε M^{-1} cm^{-1}) [b]	$E_{1/2}^{ox}$, (V) [c]
1	1906, 1831	367 (658)	−0.225
2	1910, 1836	371 (819)	−0.266
3	1908, 1936	381 (1137)	−0.297
4 [d]	1912, 1840	–	−0.340
[**1**](BF_4)	2038, 1946	372 (344), 447 (116)	–
[**2**](BF_4)	2037, 1954	415 (948), 488 (503)	–
[**3**](BF_4)	2034, 1957	424 (1470), 485 (948)	–
[**4**](PF_6) [d]	2034, 1958	–	–

[a] CH_2Cl_2 solution in 0.1 mm CaF_2 cell
[b] 0.01 M solution in CH_2Cl_2 in 0.517 mm KBr cell
[c] Pt electrode, CH_2Cl_2, 0.1 M Bu_4NPF_6, 100-200 mV/s, potentials *vs.* Fc/Fc^+ couple
[d] Experimental data for complexes $Cp(CO)_2Mn(IPr)$ (**4**) and $[Cp(CO)_2Mn(IPr)](PF_6)$ ([**4**](PF_6) retrieved from reference 16.

2, Figures S3-S5), thus being consistent with the formation of cationic complexes. UV-Vis spectroscopy investigation of the Mn^I NHC complexes **1-3** (Table 2, Figures S6-S7) show a single band in the visible region attributed to MLCT transition[26] displaying a small bathochromic shift and gradual increase of the extinction coefficient upon the replacement of the Me substituent(s) in the NHC core for Mes one(s). In contrast, all Mn^{II} NHC complexes [**1-3**](BF_4) showed two bands both shifted to the red region. Interestingly, similar trends in the position of λ_{max} and value of ε observed in the neutral Mn^I NHC species were also evidenced for both absorption bands of their cationic Mn^{II} analogues.

X-band ESR spectra of complexes [**1-3**](BF_4) in frozen solutions at 70K (Figure 3) display an anisotropic rhombic environment similar to that previously described for 17-electron neutral $[Cp(CO)_2MnXR]^{\bullet}$[27] and cationic $[Cp(CO)Mn(L)(L')]^{\bullet+}$[10c,12a,28] Mn^{II} complexes. However, we were unable to obtain g and A tensors by simple direct simulation of X-band EPR-spectra. Gratifyingly, the measurements of Q-band ESR spectra of [**2**](BF_4) at low temperature (Figure 4) combined with DFT calculations allowed us to obtain an excellent fit (Table 3). For complex [**1**](BF_4), most of the ESR features observed in frozen solution for both X- and Q-band correspond well to fitted ESR parameters optimized from starting DFT computed ones. However, some supplementary features in Q-band and X-band spectra (see asterisks in Figures 3, and 4, respectively) are clearly due to a different Mn^{II} species. Taking into account the spectroscopic and analytical purity of bulk [**1**](BF_4), we propose that a higher sensitivity of this compound to oxygen due to the low steric volume of the IMe ligand may result into its partial decomposition to form some amount of paramagnetic impurities during the preparation of highly diluted solution (0.003 M) used for the acquisition of ESR spectra.

When comparing the g tensors of the Mn^{II} cations $[\mathbf{1}]^+$ and $[\mathbf{2}]^+$, it can be seen that the highest g component (g_3) decreases significantly by $\Delta g_3 = 0.014$ from $[\mathbf{1}]^+$ to $[\mathbf{2}]^+$. Even though there is a shift between experimental and DFT computed values for the g_3 value of each complex, its variation from complex $[\mathbf{1}]^+$ to $[\mathbf{2}]^+$ is properly predicted by DFT calculations performed after geometry optimization in gas phase of [**1**](BF_4) and [**2**](BF_4), leading to $\Delta g_3 = 0.017$. This Δg_3 shift can result either from the electronic reasons due to the change of the NHC ligand from IMe ($[\mathbf{1}]^+$) to IMeMes ($[\mathbf{2}]^+$) or from a variation of conformation for the Mn–NHC fragment. In an attempt to distinguish between both contributions, we computed g_3 values for geometry-optimized structures of $[\mathbf{1}]^+$ and $[\mathbf{2}]^+$ for a given set of Cp_{cnt}–Mn1–C3–N2 dihedral angle values (Figure 5, Table S1). It was found that the amplitude of computed g_3 values for $[\mathbf{2}]^+$ was scaled down by an average factor of two when compared to that of $[\mathbf{1}]^+$. While only a small variation of g_3 value was calculated

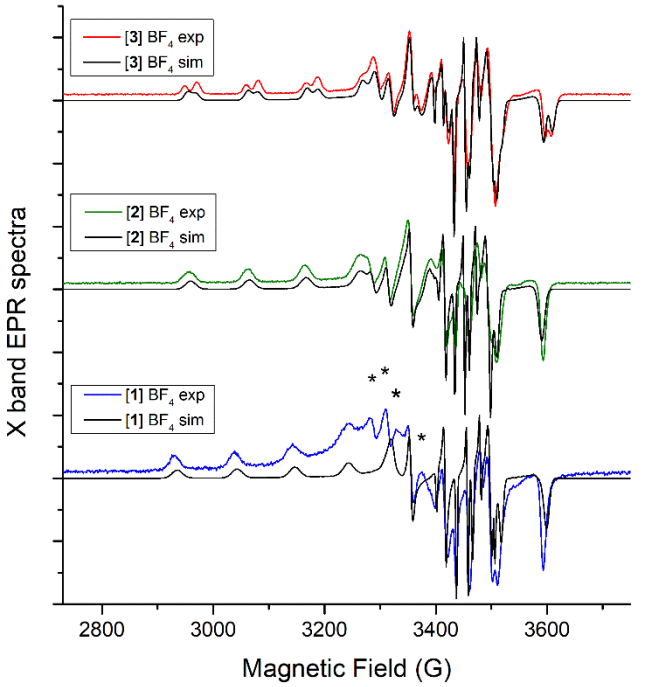

Figure 3. Experimental and simulated X-band ESR spectra of Mn^{II} NHC complexes [**1-3**](BF_4) in frozen CH_2Cl_2/toluene 1:1 mixture at 70K

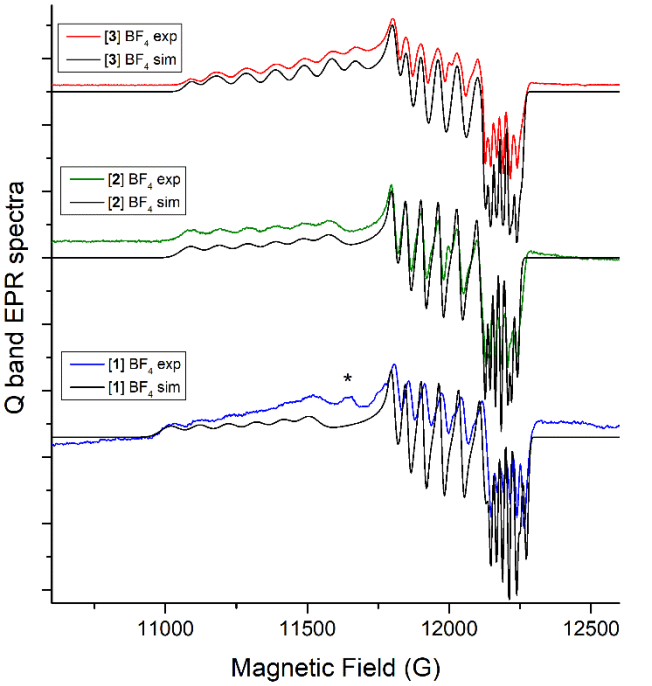

Figure 4. Experimental and simulated Q-band ESR spectra of Mn^{II} NHC complexes [**1-3**](BF_4) in frozen CH_2Cl_2/toluene 1:1 mixture at 70K.

for [**2**]$^+$ upon rotation of the NHC ligand in the −135° to −45° Cp_{cnt}–Mn1–C3–N2 dihedral angle range, a significant difference (Δg_3 = 0.017) can be noticed between horizontal ('−90°') conformers of [**1**]$^+$ and [**2**]$^+$ being close to the experimentally observed values (Δg_3 = 0.014, Table 3). It therefore appears that this Δg_3 shift between [**1**]$^+$ and [**2**]$^+$ is mainly caused by electronic factors resulting from the different nature of NHC ligands in these complexes rather than from NHC ligand orientation. Since DFT-optimized geometries for energetic minima for [**1**]$^+$ and [**2**]$^+$ remain quite close to their corresponding X-ray structures (Table 1), well-reproducing inparticular their Cp_{cnt}–Mn1–C3–N2 angles (Table 3), we expect that both conformations of [**1**]$^+$ and [**2**]$^+$ detected by ESR in frozen solution would be similar to those determined by X-ray diffraction. This may suggest that, for [**1**]BF_4 and [**2**]BF_4, internal (electronic) factors determine their conformations, more than external ones (*i.e.* crystal packing).

Table 3. Values of g and Mn hyperfine tensor components for complexes [**1-2**](BF_4) obtained from their X- and Q-band ESR spectra in frozen solution (CH_2Cl_2/toluene 1:1, 70K) and the comparison with DFT calculations data (in italic)

	[**1**]$^+$		[**2**]$^+$	
	Exp [a]	DFT [b] (*Opt/XRD*)	Exp [a]	DFT [b] (*Opt/XRD*)
g	1.995	*2.001/2.001*	1.998	*2.001/2.001*
	2.038	*2.034/2.032*	2.037	*2.032/2.036*
	2.158	*2.099/2.109*	2.144	*2.082/2.092*
Torsion Angle (°) [c]		−90.3/−88.8		−67.6/−74.1
A_{Mn}	−342	*−275/−272*	−331	*−241/−270*
	−4	*27/24*	−78	*−12/15*
	−60	*41/45*	34	*105/54*
Euler Angles (rad)	−2.84	*−2.97/−2.77*	−0.44	*−0.33/−0.47*
	1.47	*1.48/1.48*	1.87	*1.81/1.79*
	0.54	*0.44/0.45*	0.41	*0.33/0.33*

[a] Experimental ESR parameters of Mn^{II} complexes [**1**](BF_4) and [**2**](BF_4) obtained by numerical fitting of both X- and Q-band spectra using EasySpin Matlab library

[b] Calculated ESR parameters of Mn^{II} cations [**1**]$^+$ and [**2**]$^+$ obtained by DFT after geometry optimisation (Opt) in a gas phase or using directly the atom coordinates from X-ray diffraction experiments (XRD)

[c] Cp_{cnt}–Mn1–C3–N2 torsion angle

Table 4. Values of g and Mn hyperfine tensor components for two conformers of complex [**3**](BF_4) observed from its X- and Q-band ESR spectra in frozen solution (CH_2Cl_2/toluene 1:1, 70K) and the comparison with DFT calculations data (in italic)

	[**3**]$^+$ Exp		[**3**]$^+$ DFT		
	[**3a**]$^+$ [a]	[**3b**]$^+$ [a]	*Opt* [b] *'−45°'*	*Opt* [b] *'−90°'*	*XRD* [c]
g	1.997	1.998	*2.001*	*2.000*	*2.003*
	2.037	2.037	*2.030*	*2.034*	*2.042*
	2.129	2.142	*2.078*	*2.087*	*2.118*
Torsion Angle (°)[d]			*−45*	*−90*	*−82.9*
A_{Mn}	−344	−338	*−268*	*−279*	*−242*
	−66	−63	*11*	*3*	*17*
	−57	−54	*36*	*46*	*45*
Euler Angles (rad)	2.96	2.65	*2.79*	*2.66*	*2.43*
	1.41	1.28	*1.35*	*1.33*	*1.25*
	−0.49	−0.39	*−0.42*	*−0.33*	*−0.41*

[a] experimental ESR parameters of both conformations of [**3**]$^+$ were obtained by numerical fitting of both X- and Q-band spectra using EasySpin Matlab library

[b] Calculated ESR parameters of Mn^{II} cation [**3**]$^+$ obtained by DFT after geometry optimisation (Opt) *in vacuo* for fixed values of the Cp_{cnt}–Mn1–C3–N2 torsion angle

[c] using the conformation observed by X-ray diffraction ("X") for the complex [**3**]BF_4

[d] Cp_{cnt}–Mn1–C3–N2 torsion angle

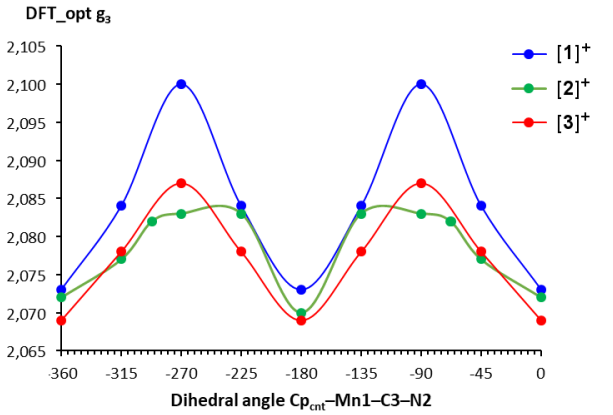

Figure 5. Plot of calculated g_3 values for geometry-optimized structures of [**1**]$^+$ (blue), [**2**]$^+$ (green) and [**3**]$^+$ (red) with constrained values of the Cp_{cnt}-Mn1-C3-N2 dihedral angles (45° step). The g_3 value for the lowest energy geometry of [**2**]$^+$ at −68° and −292° is also shown.

In contrast to complexes [**1-2**](BF_4), X-band spectrum of [**3**](BF_4) at 70K (Figure 3) reproducibly shows the presence of two sets of signals with a ratio close to 1:1 and belonging to twoclosely related paramagnetic species. Gratifyingly, the ESR spectral parameters of these compounds further denoted as [**3a**]$^+$ and [**3b**]$^+$ have been well numerically simulated (Table 4) starting from the set of parameter values provided by their DFT computation for the XRD structure (last column of Table 4). DFT calculation data show good agreement with their numerical counterparts not only in g (see Figure S10) and A tensors, but also Euler angles between them. The final numerical values yield values of g_3 components equal to 2.129 and 2.146, respectively.

Then we aimed to rationalize the origin of 0.013 difference between the g_3 values measured for [**3a**]$^+$ and [**3b**]$^+$. Though this Δg_3 value is comparable to that observed between [**1**]$^+$ and [**2**]$^+$ (0.017), in this case evidently it cannot be ascribed to electronic effects, because both species contain the same NHC ligand. We hence plot the energies of [**3**]$^+$ structures, geometry-optimized with constrained Cp_{cnt}–Mn1–C3–N2 torsion angle values (Figure S8). While the lowest energy is reached for the eclipsed conformer ('−45°'), the horizontal one ('−90°', close to [**3**]$^+$ in crystal) corresponds to a local maximum. However, the amplitude of the energy profile for [**3**]$^+$ is less than 2 kcal/mol being smaller than those computed for related complexes [**1**]$^+$ and [**2**]$^+$ (Figure S8). These data make difficult to reliably predict by DFT calculations the relative energy differences between two conformations of [**3**]$^+$ in a frozen solution and may suggest that intermolecular van der Waals forces are major players in the determination of the horizontal conformation adopted by [**3**]$^+$ in the crystal.

The calculated g_3 values for a series of constrained $[\mathbf{3}]^+$ conformers (Figure 5) show that $[\mathbf{2}]^+$ and $[\mathbf{3}]^+$ are very close (in contrast to $[\mathbf{1}]^+$), reflecting similar electronic structures due to the common presence of the Mes group in their NHC ligands. The g_3 value 2.078 computed for an eclipsed conformer ('−45°') is intermediate between those of horizontal ('−90°', 2.087) and "vertical" ('−180°', 2.069). The analysis of the plot experimental *vs.* calculated g-values for all geometry-optimized cations (Figure S10) using $[\mathbf{1}]^+$ and $[\mathbf{2}]^+$ for calibration revealed that the observed g_3 difference between both $[\mathbf{3a}]^+$ and $[\mathbf{3b}]^+$ species could indeed be ascribed to the difference between eclipsed and horizontal conformers, respectively. Though the factors favouring the existence of two distinct conformations for $[\mathbf{3}]^+$ in the frozen solution are not obvious, it may be caused by the different position of the counter-anion relative to the organometallic cation.

Despite their paramagnetic nature Mn^{II} complexes $[\mathbf{1\text{-}3}](BF_4)$ are not NMR silent and we were able to record their ^1H spectra (Figures S11-S13) and to successfully carry out signal attribution (Table 5) providing, to the best of our knowledge, the first systematic ^1H NMR study of an homogeneous series of paramagnetic NHC complexes. The stepwise replacement of the methyl group(s) in the NHC core by mesityl group(s) leads to a lower paramagnetic shift of the signals of the Cp ligands with concomitant line broadening being in all cases *ca.* 2-5 times greater than in the case of the cymantrene radical-cation $[CpMn(CO)_3]^{\bullet+}$ in CD_2Cl_2 (δ_H 22.4 ppm, $w_{½}$ 230 Hz).[10c] Interestingly, the opposite trend was observed even more strikingly for the signals of heterocyclic protons and these data are consistent with those of neutral NHC radical complexes $[Cp(CO)_2Cr(IMe)]^{\bullet}$ (δ_H 30.7 ppm, $w_{½}$ 4500 Hz)[21b] and $[Cp(CO)_2W(IMes)]^{\bullet}$ (δ_H 23.17 ppm, $w_{½}$ 300 Hz).[21a] Contrary to the Cp, N–Me, and imidazolium protons, the signals of the mesityl groups are little affected by the paramagnetic shift and typically show a smaller line broadening. Notably, *para*-CH_3 substituents are more influenced by the paramagnetic nature of Mn^{II} atom than the corresponding *ortho*-CH_3 ones, similarly to what has been observed for $[Cp(CO)_2W(IMes)]^{\bullet}$ (δ_H 7.56 *vs.* 1.84 ppm).[21a]

Table 5. ^1H NMR data for the complexes $[\mathbf{1\text{-}3}](BF_4)$ (CD_2Cl_2, 400.1 MHz, 25 °C) [a]

Complex	[**1**](BF$_4$)	[**2**](BF$_4$)	[**3**](BF$_4$)
Mn–C$_5$*H*$_5$	17.65 (~600) 5H, 13.2	16.9 (~800) 5H, 12.6	15.5 (~1050) 5H, 11.3
C*H*$_{Im\text{-}4,5}$	28.2 (~1350) 2H, 21.3	12.7 (240) 2H, 5.75 [b]	6.60 (115) 2H, –0.55
C*H*$_{Mes}$	–	7.25 (95) 2H, 0.25	7.85 (50) 4H, 0.8
N–C*H*$_3$	8.45 (~350) 6H, 4.65	8.65 (~650) 3H, 4.8	–
C*H*$_{3\ o\text{-}Mes}$	–	2.9 (~200) 6H, 1.0	2.35 (150) 12H, 0.2
C*H*$_{3\ p\text{-}Mes}$	–	6.6 (150) 3H, 4.25	5.8 (125) 6H, 5.33

[a] The data are presented as following: chemical shift δ_H (ppm) with a half-width w½ (Hz) in parenthesis, integration intensity and paramagnetic shift (Δ, ppm)
[b] Average value of δ_H for non-equivalent C*H*$_{Im\text{-}4,5}$ protons in complex **2**

Conclusions

We have shown that cationic 17-electron Mn^{II} complexes $[Cp(CO)_2Mn(NHC)](BF_4)$ bearing different NHC ligands can be easily prepared by the oxidation of the corresponding Mn^{I} precursors and display a similar stability as ferrocenium salts. The Mn^{I}/Mn^{II} redox interconversion can be easily detectable by various spectroscopic methods including among others IR spectroscopy in the carbonyl region and conventional ESR spectroscopy typically unavailable for ferrocenium cations.[29] Additionally, this investigation clearly illustrates the potential of the combination of modern ESR spectroscopy and theoretical chemistry making possible the experimental detection of subtle conformational changes in organometallic complexes and their reliable structural attribution. The ease of synthesis of $[Cp(CO)_2Mn(NHC)]$ complexes from industrially produced $[CpMn(CO)_3]$ and readily available NHCs, including their possible derivatization either by substitution of the Cp ring[30] or *via* the NHC ligand backbone[14,31] clearly opens an avenue for the application of these compounds as convenient redox active moieties in parallel to ubiquitous Fc derivatives.

Experimental

Materials and methods.

All manipulations were carried out using Schlenk techniques under an atmosphere of dry nitrogen. Dry and oxygen-free organic solvents (THF, Et_2O, CH_2Cl_2, pentane or toluene) were obtained using LabSolv (Innovative Technology) solvent purification systems. Deuterated CD_2Cl_2 used for NMR experiments was deoxygenated by three freeze-pump-thaw cycles and kept over 4Å molecular sieves. Manganese NHC complexes **1-3**[14,17] and $[Fc](BF_4)$[32] were prepared by known procedures.

Solution IR spectra were recorded in 0.1 mm CaF_2 cells using a Perkin Elmer Frontier FT-IR spectrometer with a resolution of 0.5 cm^{-1} and given in cm^{-1} with relative intensity in parentheses. UV-Vis spectra were recorded on UV-Visible Spectrometer Varian Cary 50. Paramagnetic ^1H NMR spectra were obtained on Bruker Avance 400 spectrometer and referenced to the residual signals of deuterated solvent.[33] X- and Q-band ESR spectra were obtained using Elexsys E580 spectrometer. The spectra were simulated by EasySpin 5.2.28 library running with Matlab.[34] Solid state magnetic susceptibilities μ_{eff} were determined by Squid using MPMS 5 Quantum Design magnetometer and then corrected for the diamagnetic ligands contribution.[35] Elemental analyses were carried out at the LCC-CNRS (Toulouse, France) using a Perkin Elmer 2400 series II analyzer.

Cyclic voltammetry and squarewave voltammetry studies were performed on Autolab PGSTAT100 instrument controlled by GPES 4.09 software under Ar atmosphere in CH_2Cl_2 solution using three-electrode cell consisted of a Pt working electrode (d = 0.5 mm), a platinum wire (S = 1 cm^2) as counter electrode, and a SCE electrode as a reference. 0.1 M solution of Bu_4NPF_6 was used as the supporting electrolyte and sample concentrations were 1×10^{-3} M. All peak potentials are given relative to the ferrocene/ferrocenium couple ($E_{1/2}$ = +0.46 V *vs.* SCE in CH_2Cl_2).

Synthesis of complexes [1-3]BF_4.

Solid [Fc](BF_4) (137 mg, 0.5 mmol) was added in one portion to a solution of complex **1** (136 mg, 0.5 mmol) in CH_2Cl_2 (10 mL) at 0°C. The initial yellow-orange color of the solution turned brown and then became red-orange in several minutes. The cooling bath was removed and the reaction mixture was stirred at RT for 10-15 min until full conversion of **1** was observed in IR spectrum. The volatiles were evaporated under vacuum and the residue was washed with ether (2×5 mL) to remove ferrocene. The resulting crude [**1**](BF_4) was dissolved in CH_2Cl_2 (8 mL), the solution was filtered through Celite and ether (20 mL) was added dropwise under vigorous stirring to induce the crystallization of the product. The supernatant was removed by decantation and the precipitate was washed with ether (5 mL) and dried under vacuum to afford [**1**](BF_4) (168 mg, 94%) as red crystals. Similarly, starting from complexes **2** (188 mg, 0.5 mmol) or **3** (240 mg, 0.5 mmol) and [Fc](BF_4) (137 mg, 0.5 mmol) the corresponding compounds [**2**](BF_4) (220 mg, 95%) and [**3**](BF_4) (261 mg, 92%) were obtained as red crystals and orange microcrystalline powder, respectively. Spectroscopic data for complexes [**1-3**](BF_4) are presented in Tables 2-5.

[**1**](BF_4): Anal. Found: C, 39.9; H, 3.25; N, 7.75. Calcd. for $C_{12}H_{13}BF_4MnO_2N_2$: C, 40.15; H, 3.65; N, 7.8. μ_{eff} = 2.1 μ_B.

[**2**](BF_4): Anal. Found: C, 51.8; H, 4.2; N, 6.0. Calcd. for $C_{20}H_{21}BF_4MnO_2N_2$: C, 51.9; H, 4.55; N, 6.05. μ_{eff} = 1.7 μ_B.

[**3**](BF_4): Anal. Found: C, 58.8; H, 4.8; N, 4.9. Calcd. for $C_{28}H_{29}BF_4MnO_2N_2$: C, 59.3; H, 5.15; N, 4.95. μ_{eff} = 2.2 μ_B.

Crystallographic details.

Single crystals suitable for X-ray diffraction experiments were obtained either by cooling the concentrated solution of complex **1** in ether at –20°C or by a vapor diffusion of Et_2O ([**1**](BF_4), [**3**](BF_4)) or pentane (**2**, [**2**](BF_4)) into the solutions of complexes in CH_2Cl_2 at room temperature. X-ray diffraction data were collected on a Bruker SMART / APEX II diffractometer (**1**, **2**, ([**3**](BF_4)) or on a Bruker D8/APEX II/Incoatec Mo IμS Microsource diffractometer ([**1**](BF_4)) or on a Xcalibur Sapphire2 diffractometer (complex [**2**](BF_4)) using in all cases MoKα radiation (λ = 0.71073 Å, graphite monochromator). Crystal and structure refinement details are given in the Table S2. All calculations were performed on a PC compatible computer using the WinGX system.[36] The structures were solved using the SIR92 program,[37] which revealed in each instance the position of most of the non-hydrogen atoms. All the remaining non-hydrogen atoms were located by the usual combination of full matrix least-squares refinement and difference electron density syntheses using the SHELX program.[38] Atomic scattering factors were taken from the usual tabulations. Anomalous dispersion terms for the Mn atoms were included in Fc. All non-hydrogen atoms were allowed to vibrate anisotropically. The hydrogen atoms were set in idealized positions (R_3CH, C–H = 0.96 Å; R_2CH_2, C–H = 0.97 Å; RCH_3, C–H = 0.98 Å; C(sp^2)–H = 0.93 Å; U_{iso} 1.2 or 1.5 times greater than the Ueq of the carbon atom to which the hydrogen atom is attached) and their positions refined as "riding" atoms. Complex [**1**](BF_4) was refined as inversion twin with *ca.* 48/52 component contributions. After completing the initial structure solution of complex [**3**](BF_4), it was found that *ca.* 17% of the total cell volume was filled with disordered solvent accounting for 263 electrons per unit cell, which, however, could not be well modelled in terms of atomic sites. The SQUEEZE procedure[39] was therefore applied to the data to remove this contribution consistent with a presence of one molecule of diethyl ether per complex [**3**](BF_4). CCDC 1485213 (previously reported complex **3**[20]) and 2092735-2092739 contain the supplementary crystallographic data for the structures unveiled in this paper. These data can be obtained free of charge from the Cambridge Crystallographic Data Centre via www.ccdc.cam.ac.uk/data_request/cif.

DFT calculations.

Geometry optimization of the Mn^{II} complexes [**1-3**]$^+$ was performed *in vacuo* with the DFT-ADF (Amsterdam Density Functional) code developed by E. J. Baerends and co-workers[40] using triple-zeta basis sets (TZ2P).[41] We relied on the Generalized Gradient Approximation (GGA) VBP exchange-correlation (XC) potential (VWN + BP: Vosko, Wilk and Nusair,[42] corrective terms by Becke[43] for the exchange and Perdew[44] for the correlation) with ADF grid precision 6. Calculations of the g-tensors of the Mn^{II} radical cations were accomplished with the same XC potential using the relativistic (full spin-orbit) two-component Zeroth-Order Regular Approximation (ZORA)[45] option and quadrupole-zeta basis sets (QZ4P).[41]

Conflicts of interest

There are no conflicts to declare.

Acknowledgements

We thank the Centre National de la Recherche Scientifique (CNRS, France) and the French national EPR facilities network (IR RENARD CNRS 3443) for a general support of this work. R.B. is grateful to French MENESR for a PhD fellowship. D.A.V. thanks the IDEX-UNITI for a starting grant.

Notes and references

1 (*a*) P. D. Beer, *Acc. Chem. Res.*, 1998, **31**, 71; (*b*) R. Sun, L. Wang, H. Yu, Z. Abdin, Y. Chen, J. Huang and R. Tong, *Organometallics*, 2014, **33**, 4560.

2 (*a*) C. M. Casado, I. Cuadrado, M. Moran, B. Alonso, B. Garcia, B. Gonzalez and J. Losada, *Coord. Chem. Rev.*, 1999, **185-186**, 53; (*b*) B. Fabre, *Chem. Rev.*, 2016, **116**, 4808; (*c*) A. Khan, L. Wang, H. Yu, M. Haroon, R. S. Ullah, A. Nazir, T. Elshaarani, M. Usman, S. Fahad and F. Haq, *Appl. Organometal. Chem.*, 2018, **32**, e4585.

3 (*a*) S. Ø. Scottwell and J. D. Crowley, *Chem. Commun.*, 2016, **52**, 2451; (*b*) X. Liu, A. Rapakousiou, C. Deraedt, R. Ciganda, Y. Wang, J. Ruiz, H. Gu and D. Astruc, *Chem. Commun.* 2020, **56**, 11374.

4 (*a*) P. Nguyen, P. Gomez-Elipe and I. Manners, *Chem. Rev.*, 1999, **99**, 1515; (*b*) R. Pietschnig, *Chem. Soc. Rev.*, 2016, **45**, 5216; (*c*) M. Gallei and C. Ruettiger, *Chem. Eur. J.*, 2018, **24**, 10006.

5 (*a*) A. M. Allgeier and C. A. Mirkin, *Angew. Chem. Int. Ed.*, 1998, **37**, 894; (*b*) V. Blanco, D. A. Leigh and V. Marcos, *Chem.*

Soc. Rev., 2015, **44**, 5341; (*c*) C. Chen, *ACS Catal.*, 2018, **8**, 5506; (*d*) J. Wei and P. L. Diaconescu, *Acc. Chem. Res.*, 2019, **52**, 415; (*e*) Y. Ryu, G. Ahumada and C. W. Bielawski, *Chem. Commun.*, 2019, **55**, 4451.

6 Selected examples: (*a*) I. M. Lorkovic, R. R. Duff and M. S. Wrighton, *J. Am. Chem. Soc.,* 1995, **117**, 3617; (*b*) C. K. A. Gregson, V. C. Gibson, N. J. Long, E. L. Marshall, P. J. Oxford and A. J. P. White, *J. Am. Chem. Soc.,* 2006, **128**, 7410; (*c*) E. M. Broderick, N. Guo, T. Wu, C. S. Vogel, C. Xu, J. Sutter, J. T. Miller, K. Meyer, T. Cantat and P. L. Diaconescu, *Chem. Commun.,* 2011, **47**, 9897; (*d*) E. M. Broderick, N. Guo, C. S. Vogel, C. Xu, J. Sutter, J. T. Miller, K. Meyer, P. Mehrkhodavandi and P. L. Diaconescu, *J. Am. Chem. Soc.,* 2011, **133**, 9278; (*e*) R. Savka, S. Foro, M. Gallei, M. Rehahn and H. Plenio, *Chem. Eur. J.*, 2013, **19**, 10655; (*f*) K. Arumugam, C. D. Varnado, S. Sproules, V. M. Lynch and C. W. Bielawski, *Chem. Eur. J.*, 2013, **19**, 10866; (*g*) L. Hettmanczyk, S. Manck, C. Hoyer, S. Hohloch and B. Sarkar, *Chem. Commun.*, 2015, **51**, 10949; (*h*) P. Neumann, H. Dib, A.-M. Caminade and E. Hey-Hawkins, *Angew. Chem. Int. Ed.*, 2015, **54**, 311; (*i*) M. Chen, B. P. Yang and C. L. Chen, *Angew. Chem. Int. Ed.*, 2015, **54**, 15520; (*j*) L. A. Brown, J. L. Rhinehart and B. K. Long, *ACS Catal.*, 2015, **5**, 6057; (*k*) L. Hettmanczyk, L. Suntrup, S. Klenk, C. Hoyer and B. Sarkar, *Chem. Eur. J.*, 2016, **23**, 576; (*l*) A. Straube, P. Coburger, L. Dütsch and E. Hey-Hawkins, *Chem. Sci.,* 2020, **11**, 10657.

7 According to IUPAC recommendations, Fc is chosen as a reference for electrochemistry in non-aqueous solutions, see: G. Gritzner and J. Kuta, *Pure Appl. Chem.*, 1984, **56**, 461.

8 A. Togni and T. Hayashi, *Ferrocenes: Homogeneous Catalysis, Organic Synthesis, Material Science*; VCH: Weinheim, 1995.

9 F. Paul and C. Lapinte, *Coord. Chem. Rev.*, 1998, **178–180**, 431.

10 (*a*) L. I. Denisovich, N. V. Zakurin, S. P. Gubin and A. G. Ginzburg, *J. Organomet. Chem.*, 1975, **101**, C43; (*b*) C. J. Pickett and D. Pletcher, *J. Chem. Soc. Dalton Trans.*, 1976, 636; (*c*) D. R. Laws, D. Chong, K. Nash, A. L. Rheingold and W. E. Geiger, *J. Am. Chem. Soc.*, 2008, **130**, 9859.

11 K. Wu, S. Top, E. A. Hillard, G. Jaouen and W. E. Geiger, *Chem. Commun.*, 2011, **47**, 10109.

12 (*a*) N. G. Connelly and M. D. Kitchen, *J. Chem. Soc. Dalton Trans.*, 1977, 931; (*b*) J. W. Hershberger, R. J. Klingler and J. K. Kochi, *J. Am. Chem. Soc.*, 1983, **105**, 61; (*c*) J. K. Kochi, *J. Organomet. Chem.* 1986, **300**, 139; (*d*) Y. Huang, G. B. Carpenter, D. A. Sweigart, Y. K. Chung and B. Y. Lee, *Organometallics*, 1995, **14**, 1423.

13 M. J. Saw and W. E. Geiger, *Organometallics*, 1996, **15**, 13.

14 A. A. Grineva, D. A. Valyaev, V. César, O. A. Filippov, V. N. Khrustalev, S. E. Nefedov and N. Lugan, *Angew. Chem. Int. Ed.,* 2018, **57**, 7986.

15 (*a*) M. N. Hopkinson, C. Richter, M. Schedler and F. Glorius, *Nature*, 2014, **510**, 485; (*b*) S. Roy, K. C. Mondal and H. W. Roesky, *Acc. Chem. Res.*, 2016, **49**, 357; (*c*) V. Nesterov, D. Reiter, P. Bag, P. Frisch, R. Holzner, A. Porzelt and S. Inoue, *Chem. Rev.*, 2018, **118**, 9678; (*d*) Y. Kim and E. Lee, *Chem. Eur. J.*, 2018, **24**, 19110.

16 K. Wu, M. A. Conger, R. Waterman, M. Liptak and W. E. Geiger, *Polyhedron*, 2019, **157**, 442.

17 J. Zheng, S. Elongovan, D. A. Valyaev, R. Brousses, V. César, J.-B. Sortais, C. Darcel, N. Lugan and G. Lavigne, *Adv. Synth. Catal.*, 2014, **356**, 1093.

18 Experimental Tolman Electronic Parameter (TEP) values for IMe and IMes are 2053 and 2051 cm^{-1}, respectively, see: H. V. Huynh, *Chem. Rev.*, 2018, **118**, 9457.

19 (*a*) T. Dröge and F. Glorius, *Angew. Chem. Int. Ed.*, 2010, **49**, 6940; (*b*) D. J. Nelson and S. P. Nolan, *Chem. Soc. Rev.*, 2013, **42**, 6723.

20 X-ray structure of complex **3** (CCDC 1485213) was previously published by some of us, see: D. A. Valyaev, M. A. Uvarova, A. A. Grineva, V. César, S. N. Nefedov and N. Lugan, *Dalton Trans.,* 2016, **45**, 11953.

21 (*a*) J. A. S. Roberts, J. A. Franz, E. F. van der Eide, E. D. Walter, J. L. Petersen, D. L. DuBois and R. M. Bullock, *J. Am. Chem. Soc.*, 2011, **133**, 14593; (*b*) E. F. van der Eide, M. L. Helm, E. D. Walter and R. M. Bullock, *Inorg. Chem.*, 2013, **52**, 1591.

22 (*a*) N. A. Cooley, K. A. Watson, S. Fortier and M. C. Baird, *Organometallics*, 1986, **5**, 2563; (*b*) M. C. Baird, *Chem. Rev.*, 1988, **88**, 1217; (*c*) S. Fortier, M. C. Baird, K. F. Preston, J. R. Morton, T. Ziegler, T. J. Jaeger, W. C. Watkins, J. H. MacNeil and K. A. Watson, *J. Am. Chem. Soc.*, 1991, **113**, 542.

23 K. G. Caulton, *Coord. Chem. Rev.,* 1981, **38**, 1.

24 M. D. Bala and M. I. Ikhile, *J. Mol. Catal. A.*, 2014, **385**, 98.

25 (*a*) D. A. Valyaev, R. Brousses, N. Lugan, I. Fernández and M. A. Sierra, *Chem. Eur. J.,* 2011, **17**, 6602; (*b*) V. César, L. C. Misal Castro, T. Dombray, J.-B. Sortais, C. Darcel, S. Labat, K. Miqueu, J.-M. Sotiropoulos, R. Brousses, N. Lugan and G. Lavigne, *Organometallics,* 2013, **32**, 4643; (*c*) A. A. Grineva, O. A. Filippov, Y. Canac, J.-B. Sortais, S. E. Nefedov, N. Lugan, V. César and D. A. Valyaev, *Inorg. Chem.*, 2021, **60**, 4015.

26 P. J. Giordano and M. S. Wrighton, *Inorg. Chem.*, 1977, **16**, 160.

27 (*a*) D. Sellmann, J. Müller and P. Hofmann, *Angew. Chem., Int. Ed. Engl.*, 1982, **21**, 691; (*b*) A. Winter, G. Huttner, L. Zsolnai, P. Kroneck and M. Gottlieb, *Angew. Chem., Int. Ed. Engl.,* 1984, **23**, 975; (*c*) A. Winter, G. Huttner, M. Gottlieb and I. Jibril, *J. Organomet. Chem.,* 1985, **286**, 317; (*d*) D. Sellmann and J. Müller, *J. Organomet. Chem.,* 1985, **281**, 249; (*e*) P. Lau, H. Braunwarth, G. Huttner, D. Günauer, K. Evertz, W. Imhof, C. Emmerich and L. Zsolnai, *Organometallics,* 1991, **10**, 3861; (*f*) J. W. Kee, T. S. Chwee, X. Y. Tan, R. D. Webster and W. Y. Fan, *Organometallics,* 2013, **32**, 4359; (*g*) E. S. Kelbysheva, L. N. Telegina, T. V. Strelkova, M. G. Ezernitskaya, A. F. Smol'yakov, Y. A. Borisov, B. V. Lokshin, E. A. Konstantinova, O. I. Gromov, A. I. Kokorin, and N. M. Loim, *Organometallics*, 2019, **38**, 2288.

28 (*a*) R. D. Pike, A. L. Rieger and P. H. Rieger, *J. Chem. Soc. Faraday Trans. 1*, 1989, **85**, 3913; (*b*) M. P. Castellani, N. G. Connelly, R. D. Pike, A. L. Rieger and P. H. Rieger, *Organometallics*, 1997, **16**, 4369; (*c*) D. I. Bezuidenhout, B. van der Westhuizen, P. J. Swarts, T. Chatturgoon, O. Q. Munro, I. Fernández and J. C. Swarts, *Chem. Eur. J.,* 2014, **20**, 4974.

29 Generally ferrocenium cations are ESR active only at very low temperatures (10-20K), see: (*a*) R. Prins and F. J. Reinders, *J. Am. Chem. Soc.*, 1969, **91**, 4929; (*b*) R. Prins, *Mol. Phys.*, 1970, **19**, 603; (*c*) R. Prins and A. R. Korswagen, *J. Organomet. Chem.*, 1970, **25**, C74; (*d*) R. Prins and A. G. T. G. Kortbeek, *J. Organomet. Chem.*, 1971, **33**, C33.

30 A. G. Ginzburg, *Russ. Chem. Rev.*, 1993, **62**, 1025.

31 A. A. Grineva, O. A. Filippov, S. E. Nefedov, N. Lugan, V. César and D. A. Valyaev, *Organometallics*, 2019, **38**, 2330.

32 N. G. Connelly and W. E. Geiger, *Chem. Rev.*, 1996, **96**, 877.

33 G. R. Fulmer, A. J. M. Miller, N. H. Sherden, H. E. Gottlieb, A. Nudelman, B. M. Stoltz, J. E. Bercaw and K. I. Goldberg, *Organometallics*, 2010, **29**, 2176.

34 S. Stoll and A. Schweiger, *J. Magn. Reson.*, 2006, **178**, 42.

35 G. A. Bain and J. F. Berry, *J. Chem. Educ.*, 2008, **85**, 532.

36 L. J. Farrugia, *J. Appl. Crystallogr.*, 2012, **45**, 849.

37 A. Altomare, G. Cascarano, C. Giacovazzo and A. Guagliardi, *J. Appl. Crystallogr.*, 1994, **27**, 435.

38 G. M. Sheldrick, *Acta Crystallogr.*, 2015, **A71**, 3.

39 P. v. d. Sluis and A. L. Spek, *Acta Crystallogr.*, 1990, **A46**, 194.

40 G. T. Velde and E. J. Baerends, *J. Comput. Phys.*, 1992, **99**, 84.

41 (*a*) E. van Lenthe and E.J. Baerends, J. Comput. Chem., 2003, 24, 1142; (*b*) D.P. Chong, E. van Lenthe, S. J. A. van Gisbergen and E. J. Baerends, J. Comput. Chem., 2004, **25**, 1030; (*c*) D. P. Chong, *Mol. Phys.*, 2005, **103**, 749.

42 S. H. Vosko, L. Wilk and M. Nusair, *Can. J. Phys.*, 1980, **58**, 1200.
43 A. D. Becke, *Phys. Rev. A*, 1988, **38**, 3098.
44 J. P. Perdew, *Phys. Rev. B*, 1986, **33**, 8822.
45 E. van Lenthe, A. E. Ehlers and E. J. Baerends, *J. Chem. Phys.*, 1999, **110**, 8943.